Modeling ocean-bottom seismic rotation rates

Ohad Barak and Shuki Ronen

ABSTRACT

Seismic systems today record up to four components which provide the particle displacement and the pressure. The pressure is proportional to the divergence of the displacement. We need the hydrophones because the divergence is useful and cannot be calculated in processing. The curl cannot be calculated from four component data just like the divergence cannot be directly calculated from the displacements. If the curl is useful, we can add rotation sensors to today's four component recorders and have seven component data.
To evaluate the added information that would come from rotation sensors we used elastic modeling. In our synthetic data experiment, we predicted the effect of a seabed scatterer on fully multi-component data. We used a pressure source that generates P waves. The P-waves are converted to S-waves and to surface waves propagating on the seabed. Our evaluation is that the added information from rotation sensors will be useful for identifying and separating surface waves from body waves.

INTRODUCTION

Four-component ocean-bottom seismic sensors (Figure 1) are a combination of a hydrophone and three-component geophones that measure linear particle velocity. The hydrophone records pressure changes in the water, and is ideally coupled to the water. It picks up mostly P-waves. The geophones are coupled to the sea-bed, and record particle velocities relating to all wave modes: P, S, and surface waves. The multiplicity of wave modes recorded by the geophones can be problematic for later sesimic processing stages, which assume a single wave mode recording (i.e., imaging with P-wave or S-wave data only). It is therefore desirable to be able to separate different wave modes within the data.

The divergence of particle motion is a spatial derivative. If we knew the displacement values everywhere within the seismic volume, then we could calculate the divergence. However, receiver stations are usually too sparse in relation to the acquired wavelengths to calculate the divergence, and in any case are always spread along a single surface (the sea bottom). The value of the divergence is not redundant even if we measure the three components of the displacement, since it can be used to detect the propagation direction of the waves incident on the sea bottom (upward or downward). The pressure that the hydrophone records is proportional to the di-

vergence of the particle displacements, and is therefore used for upgoing/downgoing wavefield separation.

Similar to the divergence, we can measure the rotation of particle motion by calculating the curl of the displacements. As with the divergence, curl is a spatial derivative operator, and insufficient sampling of the waves in the field can inhibit its direct calculation. However, a recently-proposed rotation sensor can be used to measure the rotation "in place". A rotation sensor measures the rotation rate (radians/unit time) of the ground at the receiver location. Similar to linear motion, the rotational motion has three components: roll, pitch and yaw. Figure 2 illustrates these motion components.

There are implementations of rotational seismic recording for earthquake seismology (Lee et al., 2009) employing ring lasers. However, these instruments are large and expensive, and are therefore not applicable to exploration acquisition. There have also been attempts to record rotational seismic data with a "Rotaphone": conventional geophones arranged along a circle (Brokesova and Malek, 2010). Newer technologies are currently under development to make rotational sensors a viable option for seismic acquisition systems. The interested reader can go to http://www.rotational-seismic.org for more information on this acquisition technology.

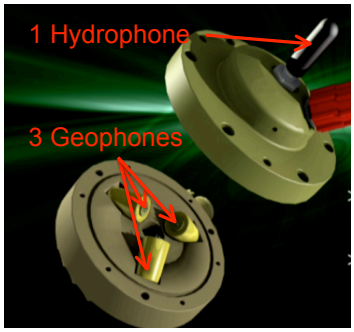

Figure 1: An example of a 4 component receiver package. One hydrophone and three geophones provide (after correction for the instrument response) the pressure of the water and the velocity of the sensor package, which is ideally coupled to the seabed. The particle velocity is the time derivative of the displacement vector, and the pressure is proportional to the divergence of the displacement, which is a spatial derivative. [**NR**]

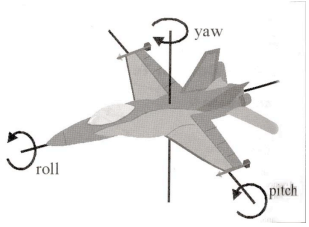

Figure 2: To know what an aircraft is doing, it is not sufficient to know its linear velocity but also the rotations. There are three components to the velocity, and in addition there are three components to the rotation: roll, pitch, and yaw. [**NR**]

The purpose of this paper is to estimate what kind of rotational motion we may expect in a simple model of ocean-bottom acquisition. We also want to show that additional information about the wave types can be acquired by having rotational motion data.

THEORY

The elastic isotropic wave equation has two state variables: the stress tensor and the particle velocity vector. The particle velocities are propagated by:

$$\partial_i \sigma_{ii} + \partial_j \sigma_{ij} + f_i(\mathbf{x}, t) = \rho \partial_t v_i, \tag{1}$$

where σ_{ii} are the normal stresses, σ_{ij} are the transverse stresses, f_i is a particle velocity force function in direction i, $\mathbf{x}$ is the spatial source location operating at time t, ρ is density and v_i is the particle velocity in direction i. The stresses are propagated using the stress-displacement relation:

$$\begin{aligned} \partial_t \sigma_{ii} &= (\lambda + 2\mu)\partial_i v_i + \lambda \partial_j v_j + f^P(\mathbf{x}, t), \\ \partial_t \sigma_{ij} &= \mu \left(\partial_j v_i + \partial_i v_j \right), \end{aligned} \tag{2}$$

where λ and μ are the Lamé elastic constants and f^P is a pressure force function. The pressure force is added equally to the normal stresses to generate a P-wave source.

We use the staggered time grid methodology for elastic propagation (Virieux, 1986), in which the stresses and particle velocities are half a time step apart. Therefore equations 1 and 2 are solved in alternation during the propagation.

The divergence of particle displacements is proportional to the pressure in the medium, the proportion being the medium parameters. It is equal to the average of the normal stresses in the stress tensor:

$$P = \overline{\boldsymbol{\sigma}} = (\lambda + \mu) \nabla \cdot \vec{\mathbf{u}}, \tag{3}$$

where P is the pressure value and $\vec{\mathbf{u}}$ are the displacements. Pressure waves cause a volumetric deformation in the medium, and their value can therefore be extracted by using equation 3 on forward modeled wavefields. However, other wave types can also generate a volumetric deformation at free surfaces, as a result of the discontinuity of the stresses.

We define rotation as the first time derivative of the curl of displacements:

$$\vec{\mathbf{R}} = \partial_t \nabla \times \vec{\mathbf{u}}. \tag{4}$$

The curl operation results in the non-volumetric part of the deformation, i.e. the "shear" deformation. At a free surface, this deformation will cause a rotation. In an isotropic medium, the curl is associated with S-waves. However, at a free surface, both P-waves and surface waves will also generate non-volumetric deformation. The units we use for rotations in this paper are milliradians/second.

MODELING RESULTS

The purpose of the modeling we ran was to synthesize ocean-bottom seismic acquisition, therefore we used a simple 2-layer model of water over solid. The source was at the water surface, and receivers were at the water bottom. We executed two runs: one with a near-seabed anomaly, and one without. The anomaly generated scattering of both P and S waves, which upon interacting with the seabed also gave rise to a seabed interface wave. The model without the anomaly enabled us to see which part of the wavefield was due to the scattering. The V_p velocity models used are shown in Figures 3(a) and 3(b). The parameters of the two layers were:

1. $V_{p1} = 1.5\,\mathrm{km/s},\ V_{p2} = 1.6\,\mathrm{km/s}.$
2. $V_{s1} = 0\,\mathrm{km/s},\ V_{s2} = 0.6\,\mathrm{km/s}.$
3. $\rho_1 = 1.025\,\mathrm{gr/cm^3},\ \rho_2 = 1.7\,\mathrm{gr/cm^3}.$

The anomaly was a Gaussian, which extended outward to a radius of 10 meters, and was centered 10 meters below the seabed. The medium parameters at the center of the anomaly were: $V_p = 1.75\,\mathrm{km/s}$, $V_s = 0.9\,\mathrm{kms}$, and $\rho = 2.1\,\mathrm{gr/cm^3}$. We did not do any testing with the anomaly parameters, although presumably altering these parameters would result in greater or lesser scattering. At this point, all we required was a feasible source of surface waves. A near-seabed anomaly simulates a "rock" buried just below the seabed, or the leg of a platform, either of which could be sources for scattered surface waves. Our source was a pressure source simulating an airgun, located at the water surface. The wavelet was a Ricker with 25Hz central frequency. There is no source-side ghost from the water surface, since we used an absorbing upper boundary. However, this ghost is simulated by the second lobe of the injected Ricker wavelet.

Figures 4(a) and 4(b) are snapshots of the vertical and horizontal P particle velocities of the entire wavefield at $t = 0.3$s. The incident, reflected and transmitted P-waves are prominent in these snapshots. Also visible is the transmitted S-wave, which is the conversion of the P-wave inciding on the seabed. The scattered S-wave and Scholte wave are visible as a semicircle, expanding from the anomaly location at $x = 100$m.

Figure 4(c) is the pressure as calculated by equation 3. We can see that the waves that generate most of the volumetric deformation are indeed the P-waves. However,

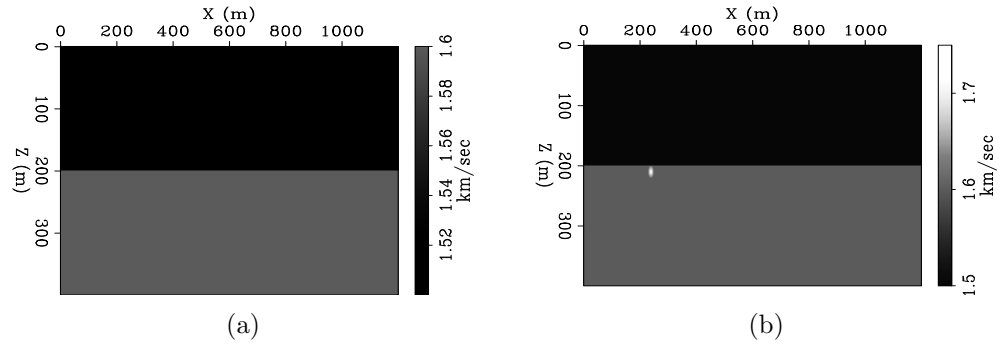

(a) (b)

Figure 3: P-wave velocity models. (a) velocity model without anomaly. (b) velocity model with anomaly. The anomaly is a Gaussian, with a diameter of 20 meters. [**ER**]

the Scholte wave also generates some volumetric deformation at the seabed. Figure 4(d) is the rotation as calculated by equation 4. The waves that generate shear deformation (and thus rotational motion at the surface) are the transmitted S-wave, and the scattered S and Scholte waves. Notice that the transmitted S-wave is coming off the P head-wave, and is therefore propagating along the seabed at P-wave velocity.

Figures 5(a)-5(d) are snapshots of the same four fields, at $t = 0.8$s. The scattered S-wave and the scattered Scholte wave are separated at this point in the propagation, since the velocity of surface waves is slightly lower than that of S-waves. The imprint of the Scholte wave on both the pressure and the rotation sections is visible.

Figures 6(a) and 6(b) are the vertical and horizontal particle displacement recordings at the seabed for the velocity model without the anomaly. Figures 6(c) and 6(d) are the pressure and rotation, respectively. The incident P-wave causes both a pressure deformation and a shear deformation at the surface, and it therefore generates a transmitted S-wave. However the moveout of the S-wave is still that of the P-wave.

Figures 7(a) and 7(b) are the vertical and horizontal particle displacement recordings at the seabed for the velocity model containing the anomaly. At $x = 1000$m, the arrivals of the direct P, scattered S and scattered Scholte wave are are marked. The S arrival is too weak compared to the P and Scholte waves to be observed in these sections. Figures 7(c) and 7(d) are the pressure and rotation recordings. We can think of these sections as the hydrophone and rotational sensor recordings. Comparing Figures 6(d) and 7(d), we can see that while most of the linear particle displacement is due to the P-wave, the Scholte wave is responsible for generating strong rotational motion.

Figures 8(a)-9(c) show the three separate arrival-time windows of each wave type. The arrival times and offset where they were extracted from are marked in Figure 7(a). Figure 8(a) is the volumetric pressure generated by the P-wave and Scholte wave arrivals, as calculated by equation 3. Figure 8(b) is the hodogram of particle displacements of those arrivals. Notice that the P hodogram is slightly elliptical,

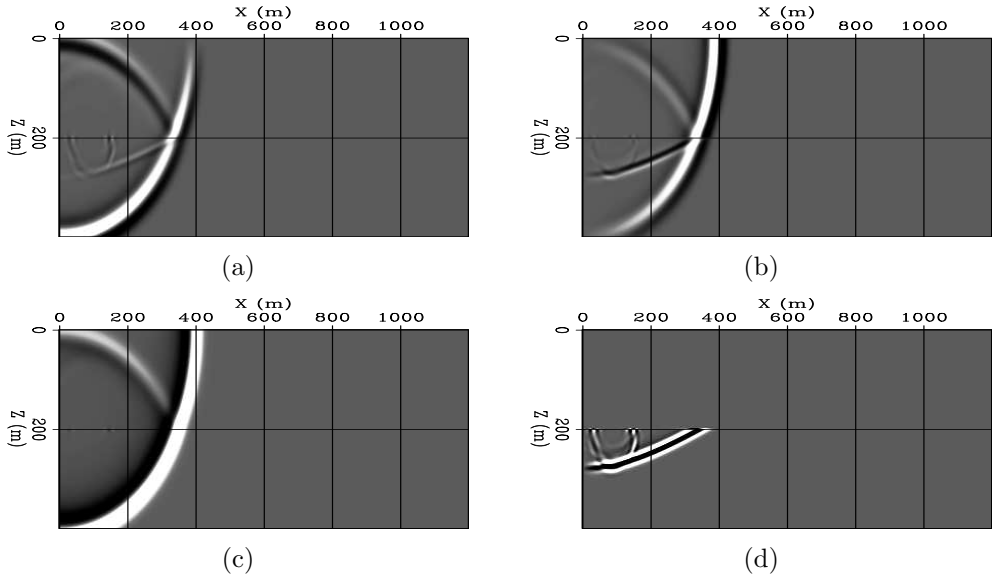

Figure 4: Wavefield snapshots at $t = 0.3$s seconds for the velocity model containing a near-surface anomaly. (a) Vertical particle velocity. (b) Horizontal particle velocity. (c) Pressure. (d) Rotation. The source is an airgun near the sea surface. In (a) and (b), all wave modes are present: direct P, reflected P, transmitted P and transmitted S. Also apparent are the S and Scholte waves which have scattered off the anomaly at $x = 100m$. In (c) and (d) there is separation: the S waves are not in (c) and P waves are not in (d). The surface waves are in both (c) and (d). [**ER**]

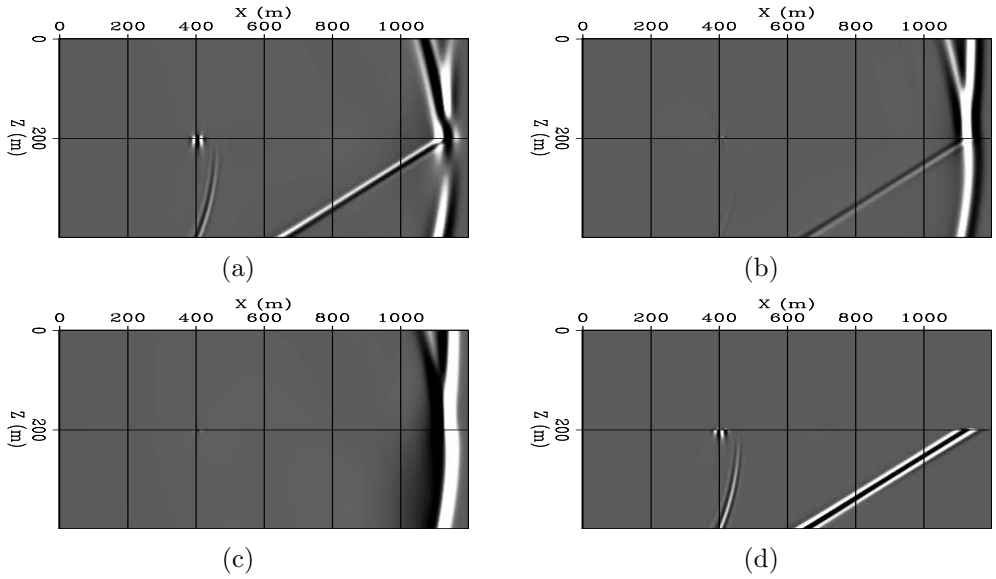

Figure 5: Wavefield snapshots at $t = 0.8$ seconds for the velocity model containing a near-surface anomaly. (a) Vertical particle velocity. (b) Horizontal particle velocity. (c) Pressure. (d) Rotation. Note how the scattered S body wave and the Scholte surface wave separate with travel time, as a result of their slightly differing velocities. Note that the Scholte wave generates both a rotational and a volumetric deformation. [**ER**]

which means that the particle motion is not linear, as it is in a body wave. The reason for that is the mode conversion which takes place when the P-wave hits the seabed. What we are seeing is a combination of P and S displacements. We can see however that the Scholte displacement hodogram is very elliptical. Figure 8(c) is the rotation rate of the P and Scholte arrivals, as calculated by equation 4. The P-wave does generate some rotational motion, and this is again a result of the mode conversion at the seabed. However, the Scholte wave generates greater rotational motion, even though the linear displacements of this wave are much weaker than those of the P-wave.

Figures 9(a)-9(c) are the pressure, displacement hodogram and rotation rate of the scattered S-wave arrival. The volumetric pressure this arrival generates is very weak compared to the P-wave, but while its displacements are 3 orders of magnitude weaker than those of the P-wave, its rotational motion is only 2 orders of magnitude weaker. Note how the hodogram is nearly perpendicular to the P-wave displacement hodogram.

Figures 10(a),10(b) and 10(c) are the ratios between the rotation rates and the absolute value of the displacement vectors of the P, S and Scholte wave arrivals. This ratio serves as a good indication as to which of the waves is a P-wave, and which are S or Scholte waves. The S and Scholte waves give rise to much more rotational motion in comparison to linear motion. P-waves, even when propagating along the

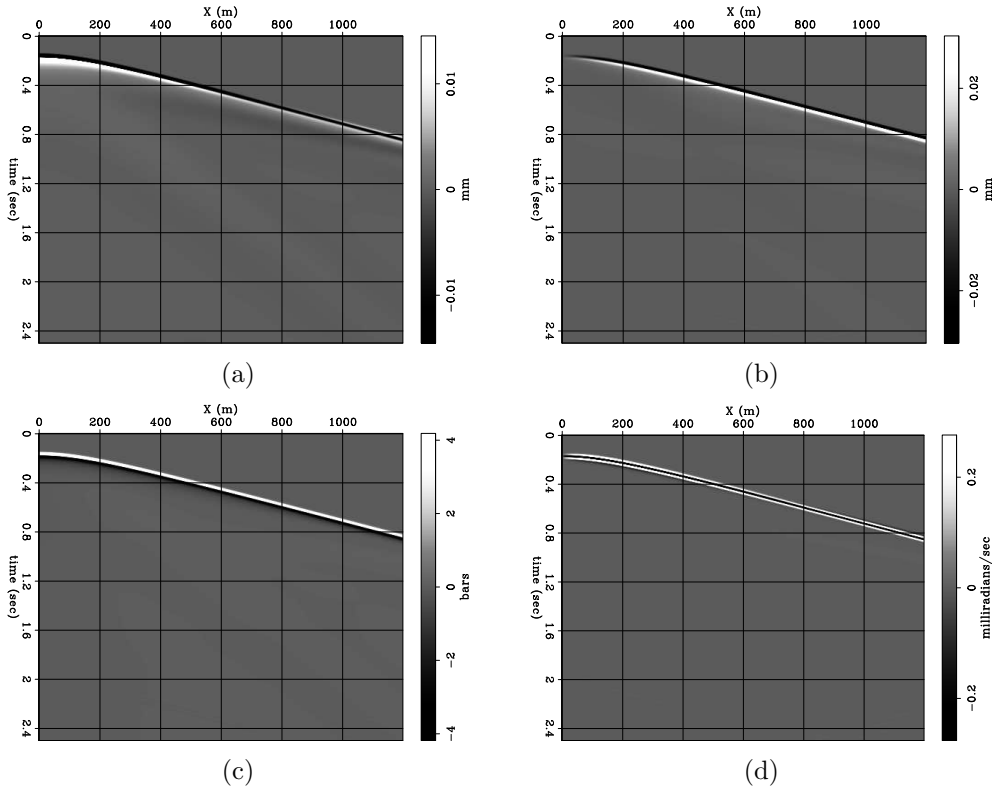

Figure 6: Synthetic data recording at sea-bottom without anomaly. (a) Vertical particle displacement. (b) Horizontal particle displacement. (c) Pressure. (d) Rotation. [**ER**]

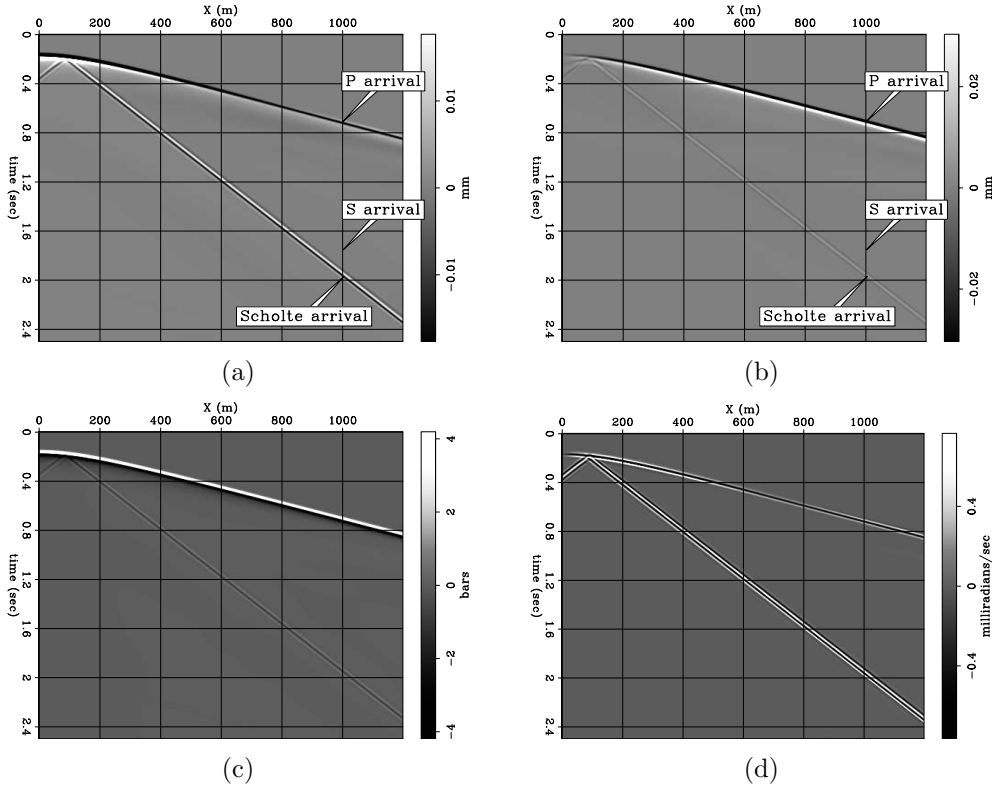

Figure 7: Synthetic data recording at sea-bottom with anomaly. The scattered Scholte wave is visible, but the scattered S-wave is relatively too weak to observe in these sections. The annotations indicate where time windows were taken for the plots in the next figure. (a) Vertical particle displacement. (b) Horizontal particle displacement. (c) Pressure. (d) Rotation. [**ER**]

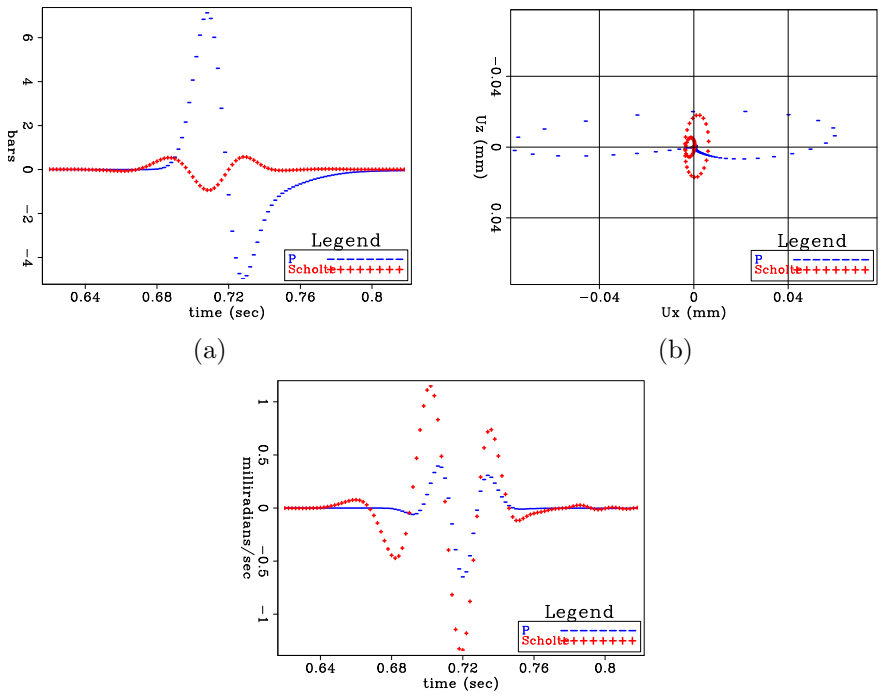

Figure 8: P and Scholte wave arrivals at the ocean-bottom receiver at $x = 1000m$, where the scattering was off the anomaly. (a) Pressure of arrivals. (b) Hodogram of displacements of arrivals. (c) Rotation rate of arrivals. Note how the P-wave has greater linear displacements compared to the Scholte wave, but a smaller rotation rate. [**ER**]

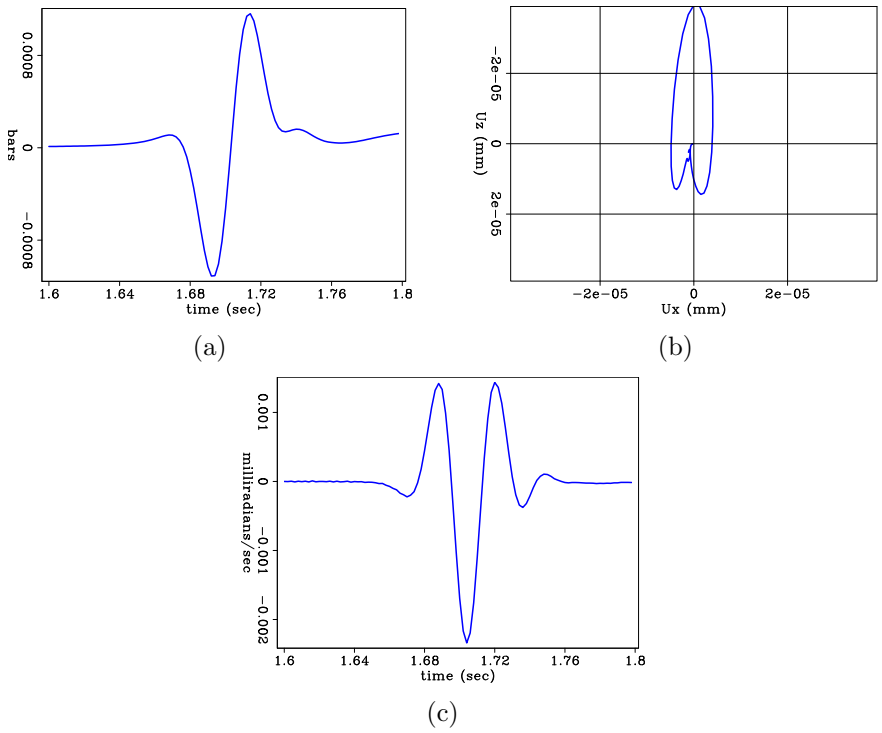

Figure 9: Shear wave arrival at the ocean-bottom receiver at $x = 1000m$, where the scattering was off the anomaly. (a) Pressure of S arrival. (b) Hodogram of displacements of S arrival. (c) Rotation rate of S arrival. [**ER**]

seabed, generate mostly linear particle motion.

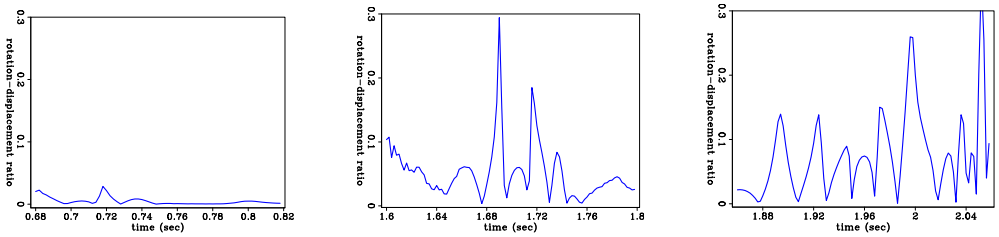

(a) (b) (c)

Figure 10: Ratio of rotation rate to absolute value of displacement for P, S and Scholte wave arrivals at the ocean-bottom receiver at $x = 1000$m, where the scattering was off the anomaly. (a) Ratio for P arrival. (b) Ratio for S arrival. (c) Ratio for Scholte wave arrival. Note that the ratio for S and Scholte waves is an order of magnitude greater than for the P wave. [**ER**]

DISCUSSION AND CONCLUSION

The main conclusion is that rotational sensors can provide us with additional information about the type of waves recorded by ocean-bottom acquisition. The key characteristic for separating between the waves is the ratio between the linear and rotational motions. At the seabed, the P-waves have a mostly linear motion. Scattered S and Scholte waves have a mostly rotational motion.

When designing a new sensor, one of the important questions is its sensitivity. Sensor sensitivity can be parameterized by over-drive level and dynamic range. A sensor that is not sensitive enough will not register weak signal. A sensor that is too sensitive will over-drive too often and will not provide useful information on high amplitude events. Depending on the electronics and the analog instrument impulse response, the time to recover from overdrive may be from a few milliseconds to a second. The dynamic range is of course limited by the analog dynamic range of the sensor and by the number of bits of the digital data (32 bits in modern emerging A/D converters which is usually way above analog dynamic range). In this paper we provide predicted numbers in terms of milliradians/sec of rotation, bars of pressure, and millimeters of displacement.

However, it is important to note that so far our study is based on 2D elastic modeling. In this paper there is circular spreading of body waves and no spreading of surface waves, which is why they do not weaken with offset. The reason we chose the offset $x = 1000$m at which to analyze the displacements was because the different arrivals were sufficiently separated there, and their different characteristics could thus be displayed. In 3D, there is spherical spreading of body waves and circular spreading of surface waves. The relation between the body-wave rotations and surface-wave rotations may be very different in 3D as a result of the added degree of freedom. We

plan to extend this study to 3D before providing sensitivity requirements for dynamic range and over-drive levels.

ACKNOWLEDGEMENTS

We thank Tim Owen, Malcolm Lansley and Bob Brune for prompting us to consider rotation sensors.

REFERENCES

Brokesova, J. and J. Malek, 2010: 2nd IWGoRS Workshop in Prague.

Lee, W. H. K., H. Igel, and M. D. Trifunac, 2009, Recent advances in rotational seismology: Seismological Research Letters, **3**, 479–490.

Virieux, J., 1986, P-Sv wave propagation in heterogeneous media: Velocity-stress finite difference method: Geophysics, **51**, 889–901.